nature nanotechnology

LETTERS

PUBLISHED ONLINE: 27 JANUARY 2013 | DOI: 10.1038/NNANO.2012.249

A subwavelength plasmonic metamolecule exhibiting magnetic-based optical Fano resonance

Farbod Shafiei[1†], Francesco Monticone[2†], Khai Q. Le[2], Xing-Xiang Liu[2], Thomas Hartsfield[1], Andrea Alù[2*] and Xiaoqin Li[1*]

The lack of symmetry between electric and magnetic charges, a fundamental consequence of the small value of the fine-structure constant[1], is directly related to the weakness of magnetic effects in optical materials[2,3]. Properly tailored plasmonic nanoclusters have been proposed recently to induce artificial optical magnetism[4–7] based on the principle that magnetic effects are indistinguishable from specific forms of spatial dispersion of permittivity at optical frequencies[1]. In a different context, plasmonic Fano resonances have generated a great deal of interest, particularly for use in sensing applications that benefit from sharp spectral features and extreme field localization[8–12]. In the absence of natural magnetism, optical Fano resonances have so far been based on purely electric effects. In this Letter, we demonstrate that a subwavelength plasmonic metamolecule consisting of four closely spaced gold nanoparticles supports a strong magnetic response coupled to a broad electric resonance. Small structural asymmetries in the assembled nanoring enable the interaction between electric and magnetic modes, leading to the first observation of a magnetic-based Fano scattering resonance at optical frequencies. Our findings are supported by excellent agreement with simulations and analytical calculations, and represent an important step towards the quest for artificial magnetism and negative refractive index metamaterials at optical frequencies[13–15].

The first demonstration of negative refractive index at microwave frequencies was based on 'artificial magnetic' resonances in a split-ring resonator[16]. However, directly translating these concepts to optical frequencies is problematic because of the modified conduction properties of metals at these frequencies, which result in saturation of their magnetic response[17]. It has been proposed[2,6,18] that a simple symmetric arrangement of nanoparticles in a planar ring geometry (Fig. 1a) or a three-dimensional cluster may support a strong magnetic response, induced by a resonant circulating displacement current instead of conduction current. This type of magnetic molecule is particularly attractive because it can be adapted easily as the unit cell of a negative-index optical metamaterial. These ideas have prompted a few recent attempts to experimentally measure magnetic plasmon resonances in nanoclusters[19–22]. In all these experiments, however, the considered clusters are larger than, or comparable to, the wavelength of operation, and this large size causes their magnetic resonance to be combined with other higher-order scattering terms and to be substantially redshifted relative to the electric dipole response of the cluster. These issues make such a metamolecule unsuitable as a building block for negative-index metamaterials.

Using advanced atomic force microscope (AFM) nanomanipulation[23–25], we assembled a four-particle nanoring with small structural asymmetries[9,22]. This nanoring exhibits strong electric and magnetic responses that overlap spectrally in the visible frequency range. The geometry of this subwavelength metamolecule was selected for three important reasons: (i) the four-particle geometry exhibits reduced radiative loss compared to odd-numbered nanorings as a result of cancellation of higher-order multipolar terms, effectively boosting its magnetic dipole response[18]; (ii) the magnetic resonance may be tuned over a wide range and spectrally overlapped with the electric dipole resonance[3]; (iii) small deviations from a perfectly symmetric ring, controllable to some degree with AFM manipulation, lead to a near-field interaction between the magnetic and electric modes, producing a magnetic-based Fano signature in the total scattering spectrum.

These concepts are illustrated in Fig. 1. A perfectly symmetric nanoring (Fig. 1a) was designed to support overlapping electric and magnetic dipole resonances at visible frequencies[12]. When excited by a local electric field, this geometry supports a broad electric dipole response. When excited by a local magnetic field, the induced circulating displacement current supports a sharper magnetic resonance centred in the same frequency range. In an ideally symmetric configuration, a time-varying electromagnetic wave would excite both orthogonal modes, which additively contribute to the total scattering cross-section without interference (Fig. 1b). However, when small asymmetries are introduced, the modes lose their orthogonality and interfere. As a direct result of symmetry breaking, the magnetic resonance creates a characteristic Fano dip in the electric dipole scattering signature, which is also reflected in the total scattering cross-section (Fig. 1c).

We used AFM nanomanipulation to assemble the nanocluster, as illustrated in Fig. 2a. Initially, gold nanoparticles with diameters of ~100 nm were randomly dispersed on a substrate. The AFM was first used to image and identify the positions of several nanoparticles located close to one another. Four nanoparticles were then assembled into a square geometry. Scattering measurements were taken using a home-built dark-field microscope (Fig. 2b). The light impinged at an incident angle of 60°, and the scattered light was collected along the normal direction to the substrate. The measured scattering spectra generally depend on the angles of incidence and collection, and the magnetic response is strongest when detected within the plane of the nanoring. Our observation position, limited by experimental constraints, does not allow direct detection of the far-field magnetic radiation. Instead, as discussed above, the magnetic mode can couple to the electric mode as a result of suitable asymmetries, affecting the overall scattering signature, including the electric dipole component, as directly observed in our measurements (Fig. 1c).

For *s*-polarized incident light, the electric field lies in the substrate plane, and it maximally excites a magnetic dipole polarized

[1]Department of Physics and Center for Complex Quantum Systems, The University of Texas at Austin, Austin, Texas 78712, USA, [2]Department of Electrical and Computer Engineering, The University of Texas at Austin, Austin, Texas 78712, USA; [†]These authors contributed equally to this work.
*e-mail: elaineli@physics.utexas.edu; alu@mail.utexas.edu

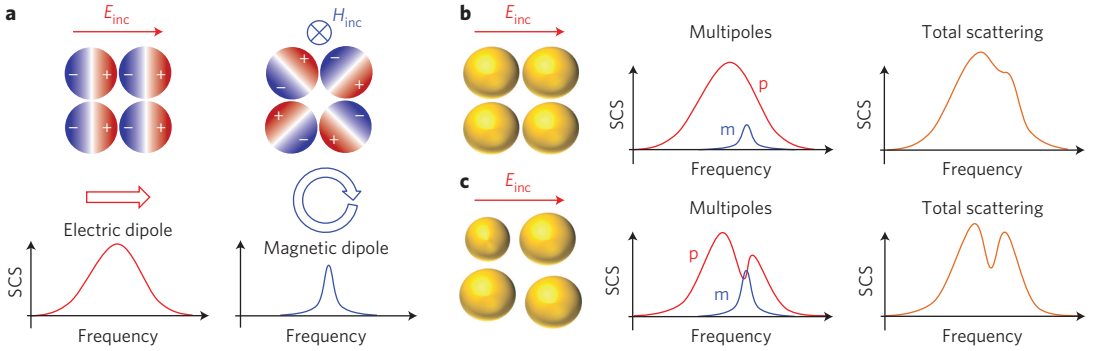

Figure 1 | Illustration of the scattering response of plasmonic nanorings. a, Scattering cross-section (SCS) of a four-particle nanoring system excited by a time-varying electric field directed along the side of the square arrangement of particles (left) and by a time-varying magnetic field directed along the normal to the plane of the nanoring (right). E_{inc} and H_{inc} represent the incident electric and magnetic fields, respectively. Colours indicate the charge distribution inside each nanoparticle. **b**,**c**, Scattering response of a symmetric nanoring (**b**) and when small asymmetries are introduced (**c**). Symmetry-breaking induces interference between the electric dipole (p) and magnetic dipole (m) modes, which gives rise to a pronounced Fano resonance in the scattering spectrum.

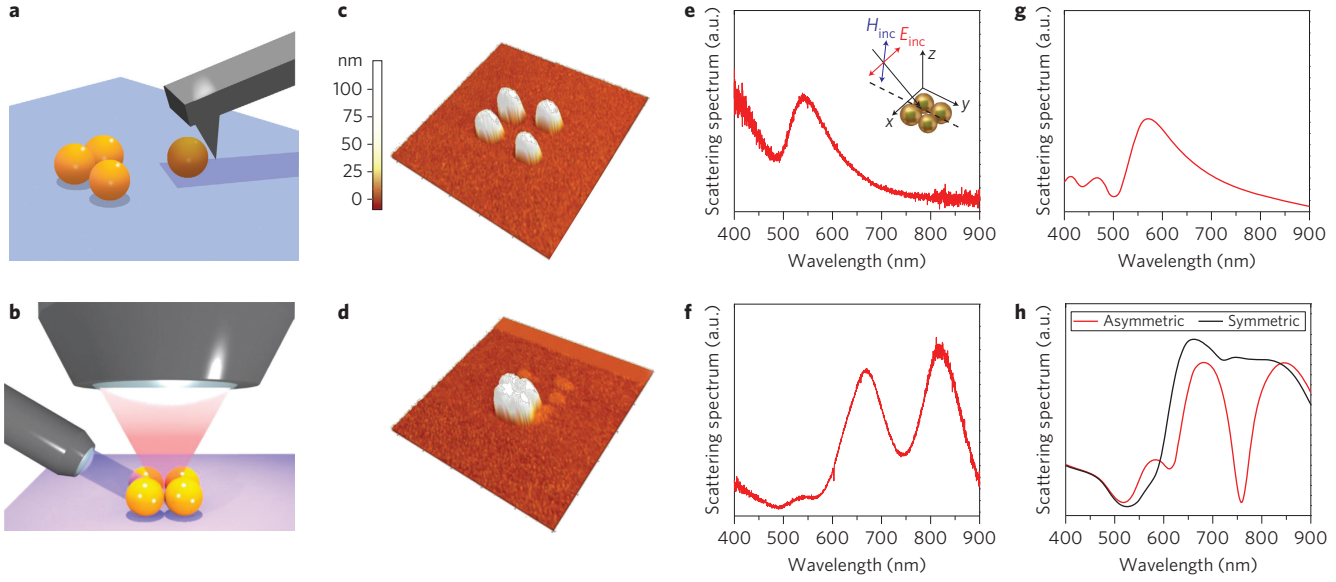

Figure 2 | Experimental set-up and scattering measurements versus simulations demonstrating the presence of a magnetic-based Fano resonance in the asymmetric nanoring. a,**b**, Schematic representations of AFM nanomanipulation (**a**) and optical scattering (**b**) set-up. **c**,**d**, AFM images of the nanorings over an area of 1.25 μm × 1.25 μm. **e**,**f**, Measured scattering spectra when the four nanoparticles are far apart (**e**) and when they are arranged in a square aggregation with small gaps (**f**). Inset in **e** illustrates the experimental geometry and corresponding coordinate system. An *s*-polarized incident light beam was used. No analyser was present along the collection path. **g**,**h**, Calculated total scattering cross-section corresponding to the geometries in **c** and **d**, respectively. Panel **h** compares the calculated scattering cross-sections for a perfectly symmetric nanoring and an asymmetric nanoring.

in the direction normal to the nanoring. When the four nanoparticles were placed far apart (Fig. 2c), the scattering spectrum with no polarizer in the collection path (Fig. 2e) was dominated by a single, broad resonance centred at 540 nm, arising from the dipole resonance of the individual nanoparticles. When the gaps between the nanoparticles were decreased, a large redshift of the electric dipole resonance was observed (Fig. 2f) due to the increased capacitive coupling between neighbouring nanoparticles. When the gap size was further reduced below 10 nm (Fig. 2d and Supplementary Fig. S2), a pronounced dip centred at 740 nm was observed (Fig. 2f). This spectral feature, quite peculiar for such a subwavelength structure, corresponds to a Fano resonance that originates from the interference between the radiant (bright), broad electric dipole and the subradiant (dark), narrow magnetic dipole modes, as illustrated in Fig. 1c. This collective plasmon response can also be interpreted in terms of hybridized states[26], for which the interference between bonding and antibonding modes gives rise to the Fano resonance.

To confirm this intuitive interpretation of the observed spectrum, we performed numerical simulations using the three-dimensional finite-element software COMSOL Multiphysics. As a starting point, we considered the geometrical parameters of the nanoring extracted from AFM images (for details see Supplementary Fig. S2) and fine-tuned their value to match the simulations to our measurements. The detailed geometry that best matched our experiment is shown in Fig. 4f (Supplementary Fig. S2). The glass substrate with refractive index $n_g = 1.5$ was included. The computed total scattering cross-sections are presented in Fig. 2g,h (red lines), and show good agreement with our measurements before and after AFM assembly. Small discrepancies between the computed and measured spectra remain and may result from a number of factors, including the difficulty in extracting precise values for gap sizes below a few nanometres, deviations from a perfect spherical shape due to surface facets (Supplementary Figs S2 and S4) and possible quantum effects due to the extremely small gap sizes[27]. However, the main features of the scattering

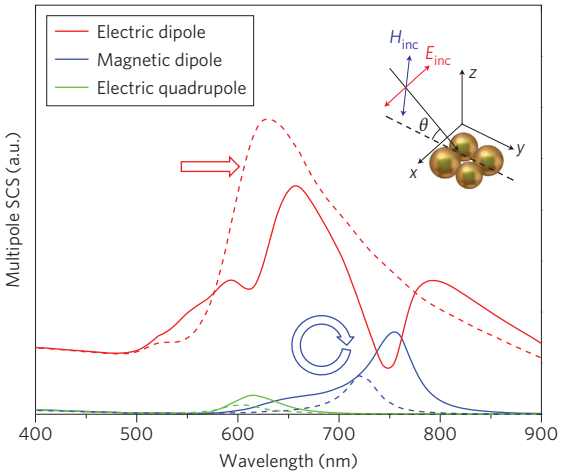

Figure 3 | Theoretical multipolar analysis of the total scattering cross-section (SCS) demonstrating the dominating magnetic dipole mode in the asymmetric nanoring. At the Fano dip (760 nm) the magnetic response is dominant in the asymmetric configuration (solid lines). Inset: geometry of the nanoring (corresponding to the structure in Fig. 2d) and coordinate system considered here. Dashed lines correspond to the symmetric nanoring.

spectra are well replicated in the simulations, validating our qualitative interpretation of the scattering spectrum and the accuracy of the numerical model. Figure 2h also shows the simulation of a similar nanoring but with uniform gap and particle size, as in Fig. 1b (we considered a sphere diameter of 100 nm and a gap size of 1.75 nm in this case). Despite the relatively small differences in geometry from the asymmetric nanoring, the simulated scattering spectrum (black line) is remarkably different. The Fano resonance completely disappears in the total scattering cross-section due to the absence of coupling between the electric and magnetic modes, consistent with our qualitative discussion and illustration in Fig. 1b. A detailed analytical study, presented in Supplementary Fig. S1, shows how small displacements of the nanoparticles in the direction of polarization of the impinging electric field, as well as small deviations in size, produce the Fano signature.

Our simulations also yield the polarization distribution inside the nanoparticles, which allows identification of the individual multipolar features associated with the measured scattering spectra. The radiation from the induced displacement currents may be described in terms of a vector potential $\mathbf{A}(\mathbf{r})$, which, in the limit of small clusters, may be expanded in quasi-static multipoles[28] as

$$\mathbf{A}(\mathbf{r}) = -i\omega\mu_0\mathbf{p}\frac{e^{ik_0 r}}{4\pi r} + \frac{i\omega\mu_0}{2}\underline{\mathbf{Q}}\cdot\nabla\frac{e^{ik_0 r}}{4\pi r} - \mu_0\mathbf{m}\times\nabla\frac{e^{ik_0 r}}{4\pi r} \quad (1)$$

where $\mathbf{p}$, $\mathbf{m}$ and $\underline{\mathbf{Q}}$ are the electric dipole, magnetic dipole and electric quadrupole moments, respectively, under the $e^{-i\omega t}$ time convention. Higher-order terms in the multipole expansion can be neglected due to the small size of the nanoparticles (see Methods for more details on the multipole expansion and calculation of the scattering cross-section contribution from each multipole). The contributions from each term are displayed in Fig. 3 on the same scale. Solid lines refer to calculations based on the realistic nanoring geometry including small asymmetries, whereas the dashed lines correspond to the ideally symmetric case. As expected, the dominant contribution is given by the electric dipole term for both scenarios. In the symmetric geometry, the electric and magnetic responses are completely uncoupled, consistent with previous theoretical studies[18]. However,

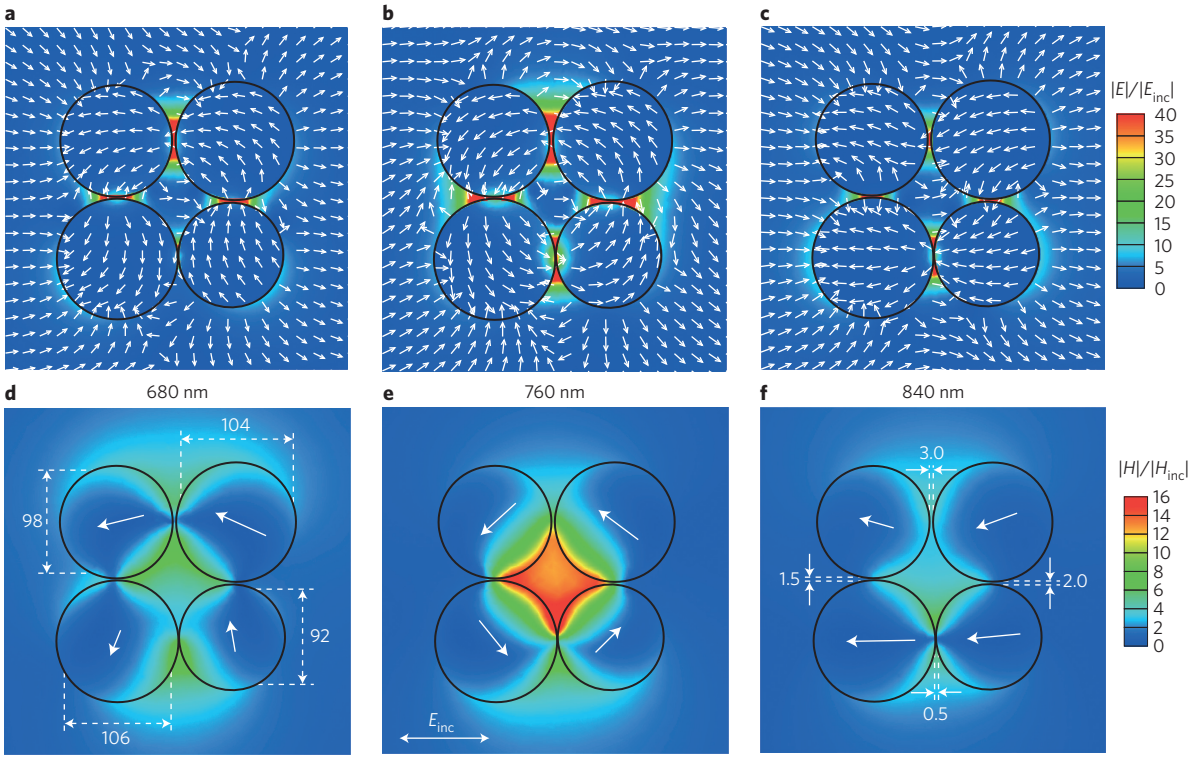

Figure 4 | Normalized electric and magnetic near-field distributions and induced electric dipole moments at different wavelengths. Top: electric field distributions and field vectors in the central plane. Bottom: magnetic field distributions and induced electric dipole moments at featured frequencies in the scattering spectra of Fig. 2f,h for the experimentally realized asymmetric nanoring. **a**,**d**, First scattering peak at 680 nm. **b**,**e**, Magnetic dipole resonance at 760 nm (dip in the scattering cross-section). **c**,**f**, Second scattering peak at 840 nm. Size of the particles and dimension of the gaps considered in the simulations are indicated in **d** and **f**, respectively. All dimensions are in nanometres. In all panels the impinging electric field is assumed to be linearly polarized as indicated in **e**.

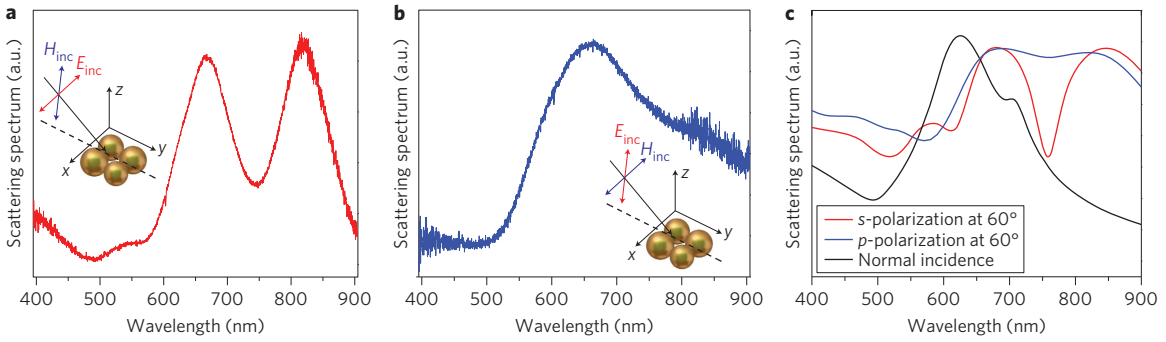

Figure 5 | Comparison between scattering spectra under different incident polarizations. a,**b**, Measured scattering spectra with *s*-polarized (**a**) and *p*-polarized (**b**) incident light. An analyser parallel to the electric field in the plane of the substrate was inserted in the path of the collected scattering signal. Insets illustrate the geometry, excitation and corresponding coordinate system. **c**, Calculated total scattering cross-section for *s*- and *p*-polarized light when the incident beam impinges with an incident angle of 60° and for the case of normal incidence (0°). A pronounced Fano dip appears only in the case of oblique incidence for *s*-polarized light.

the small asymmetries introduced in the nanoring boost the magnetic response, which acquires strength from the coupling with the electric mode and creates a strong Fano resonance at ~760 nm. At this wavelength, the electric dipolar scattering spectrum experiences a sharp drop and the magnetic dipole contribution becomes dominant. Our analysis in Fig. 3 shows that the electric quadrupolar contribution is negligible in both the symmetric and asymmetric configurations[18]. This feature is related to our choice to realize a subwavelength nanoring with an even number of nanoparticles, which reduces the undesirable radiation loss associated with the electric quadrupole mode[18]. The only residual quadrupolar component excited in the plane of the particles, Q_{xy}, in Fig. 3, makes a minor contribution to the measured scattering spectra around $\lambda_0 = 600$ nm.

Furthermore, our numerical analysis can provide a complete picture of the near-field interactions between the electric and magnetic response of the nanoring at the selected wavelengths of interest, as shown in Fig. 4. The top row of Fig. 4 shows the magnitude of the electric field distribution and the electric field vectors in the central plane of the nanoring. The bottom row shows the magnitude of the magnetic field distribution and the induced collective electric dipole moment calculated for each nanoparticle, obtained by integrating the local polarization vector. To facilitate direct comparison, the fields in each row of Fig. 4 are all plotted in the same scale. It is interesting to verify that bright 'hot spots' with highly enhanced localized fields at the gaps are obtained at the scattering dip at 760 nm (Fig. 4b). The magnetic nature of this mode is evident on inspection of the calculated circulating electric field distribution (Fig. 4b), the corresponding magnetic field distribution and the circulating electric dipole moments of the four particles (Fig. 4e). These field distributions result in a magnetic dipole moment normal to the plane of the nanoparticles. For comparison, at the two wavelengths corresponding to the scattering peaks in Fig. 2f,h, the near-field distribution is drastically different and supports a dominant electric response (left and right columns in Fig. 4).

The nanoring geometry is inherently anisotropic, and a strong magnetic response is expected only for *s*-polarized excitation. We compared the measured scattering spectra for *s*-polarized (Fig. 5a) and *p*-polarized (Fig. 5b) incident light, observing a strong reduction of the magnetic effect in the latter case. In these measurements, an analyser parallel to the electric field in the substrate plane was inserted in the path of the collected scattering signal. Our numerical calculations predict a behaviour similar to the measured spectra, as shown in Fig. 5c: the magnetic resonance contribution to the total scattering is reduced by a factor of approximately seven for *p*-polarized incident light compared with *s*-polarization light. This polarization dependence can be qualitatively understood in a simple way; only when the incident magnetic field has a significant component along the substrate normal can it excite a magnetic dipole along this direction. Our calculations further predict a similar weakening of the Fano dip for normally incident light (black line in Fig. 5c), which again does not support an out-of-plane magnetic field. A small shoulder around 700 nm is still produced by a residual magnetic dipole resonance, which may be excited at normal incidence, due to the small asymmetries of the nanoring. However, in this scenario the magnetic response and corresponding Fano effect are drastically reduced.

Our study convincingly demonstrates that a four-particle nanoring can support a strong optical magnetic resonance overlapped with a broad electric resonance. This specific geometry avoids radiative damping associated with higher-order scattering modes and boosts the magnetic response, despite the overall subwavelength size of the nanoring. In addition, the near-field interaction between the magnetic and electric modes, enabled by the small asymmetries in our geometry, has led to the first observation of a magnetic-based optical Fano resonance in the total scattering spectrum in a direction along which the direct magnetic response would otherwise be zero. AFM nanomanipulation has enabled the first realization of this novel metamolecule. Despite some challenges (for more details see Supplementary Figs S2–S4), AFM nanomanipulation allows for active modification of the nanoparticle positions, ideal for optimizing the geometry and controlling the spectral response of the metamolecule to a large degree. Other synthetic approaches, including self-assembly and electron-beam lithography, may be used to create large arrays of nanorings. Improved control over the sizes of the nanoparticle and gap may be necessary as the near-field coupling (and therefore the spectral response) of the nanoring is extremely sensitive to geometry. The uniformity in nanoparticle and gap size may be particularly crucial when periodic arrays of such metamolecules are considered. Metamaterials with engineered electric and magnetic resonances and their controlled coupling may enable many fascinating applications in nanophotonics including cloaking, high-resolution imaging, sensing and an enhanced nonlinear optical response.

Methods

Sample preparation. Photolithographical marks were deposited on a glass coverslip to locate particular areas across its surface. Nanoparticles were then deposited on this coverslip after it was cleaned using 1–2% Hellmanex-II solution for 60 min in a sonication bath at ~40 °C. Gold nanospheres (~100 nm in diameter, British Biocell 15711-20) with 5.6×10^9 particles/ml were deposited using a spin-coating procedure consisting of multiple speed steps (200, 400, 600 and 4,000 r.p.m.). To manipulate a nanoparticle, the *z* feedback of the AFM (Park Systems XE-120) was turned off. The AFM probe, following a straight line defined by the user, was moved through the centre of the nanoparticle to push the nanoparticle upon contact. Once the nanoparticle reached the target position, the tip was withdrawn and moved away from the nanoparticle. Finally, the sample was re-imaged to examine the result

of the manipulation. Although, in principle, it is possible to achieve structural control with nanometre precision using AFM nanomanipulation, the dimensions of the assembled nanoring were determined experimentally with limited accuracy (for details see Supplementary Fig. S2). The AFM probes used for both imaging and manipulation typically have a force constant of ~14 N m^{-1} (Mikromasch NSC-35-B). Typical AFM parameters used for manipulating the nanospheres are as follows: integrative gain of ~0.8, proportional gain ~0.9, servo gain ~2.0, a scanning speed of 0.35–0.5 μm s^{-1} for imaging and 2–20 μm s^{-1} for manipulation.

Scattering spectra measurements. Scattering measurements were performed using a home-built dark-field microscope (Fig. 2b). A white light source, after passing through a linear polarizer, was used to excite the nanostructures. A microscope objective with NA = 0.28 was used to focus the white light source at an incident angle of 60° to the substrate normal. An objective with NA = 0.7 was used to collect the scattering signal along the substrate normal. The scattered light was then focused onto the entrance of an imaging spectrometer and detected with a nitrogen-cooled silicon charge-coupled device. Owing to the anisotropy of the nanoring, the scattering spectra also depend on the direction of incident light. We rotated the sample such that the plane of incidence was always parallel to the sides of the square for all presented measurements.

Numerical calculations. The numerical computations were carried out by the three-dimensional finite-element software COMSOL Multiphysics. We assumed an electromagnetic plane wave impinging on the nanoring and the ring itself lying on a semi-infinite substrate with perfectly matched layer absorbing boundary conditions. Realistic values for the permittivity of gold as a function of frequency were taken from empirical data sets. The different moments in the multipole expansion were computed from the calculated distribution of polarization current $\mathbf{J} = -i\omega\mathbf{P}$, where $\mathbf{P}$ is the polarization vector inside each nanoparticle. For a non-magnetic medium, the electric dipole moment is

$$\mathbf{p} = -\frac{1}{i\omega}\int_V \mathbf{J}(\mathbf{r}')\mathrm{d}V' = \int_V \varepsilon_0(\varepsilon_\mathrm{r} - 1)\mathbf{E}(\mathbf{r}')\mathrm{d}V'$$

where V is the volume of the particle, $\mathbf{E}(\mathbf{r})$ is the electric field and ε_0, ε_r are the permittivity of vacuum and the relative permittivity of gold, respectively. The second-order terms of the expansion, that is, the magnetic dipole and electric quadrupole, are given by

$$\mathbf{m} = \frac{1}{2}\int_V \mathbf{r}' \times \mathbf{J}(\mathbf{r}')\mathrm{d}V' = -\frac{i\omega}{2}\int_V \varepsilon_0(\varepsilon_\mathrm{r} - 1)\mathbf{r}' \times \mathbf{E}(\mathbf{r}')\mathrm{d}V'$$

$$\underline{\mathbf{Q}} = -\frac{1}{i\omega}\int_V [\mathbf{J}(\mathbf{r}')\mathbf{r}' + \mathbf{r}'\mathbf{J}(\mathbf{r}')]\mathrm{d}V'$$

$$= \int_V \varepsilon_0(\varepsilon_\mathrm{r} - 1)[\mathbf{E}(\mathbf{r}')\mathbf{r}' + \mathbf{r}'\mathbf{E}(\mathbf{r}')]\mathrm{d}V'$$

The relative contributions to the total average power radiated by each multipole are then obtained by integrating the complex Poynting vector in the far-field. The closed-form solutions for the radiated powers are

$$\langle W_{\mathrm{rad},p}\rangle = \frac{k_0^4}{12\pi\,\eta_0\,\varepsilon_0^2}|\mathbf{p}|^2$$

$$\langle W_{\mathrm{rad},m}\rangle = \frac{k_0^4\,\eta_0}{12\pi}|\mathbf{m}|^2$$

$$\langle W_{\mathrm{rad,Q}}\rangle = \frac{k_0^6}{40\pi\,\eta_0\,\varepsilon_0^2}\|\underline{\mathbf{Q}}\|^2$$

where η_0 is the impedance of free space. Finally, the scattering cross-section contribution from each multipole is simply computed by normalizing to the incident power density. The total scattering cross-section of the nanoring can then be obtained by summing the scattering cross-section contributions from each multipole.

Received 10 September 2012; accepted 6 December 2012; published online 27 January 2013; corrected after print 1 February 2013

References

1. Landau, L. D. & Lifshitz, E. M. *Electrodynamics of Continuous Media* (Pergamon, 1960).
2. Alu, A. & Engheta, N. The quest for magnetic plasmons at optical frequencies. *Opt. Express* **17,** 5723–5730 (2009).
3. Merlin, R. Metamaterials and the Landau–Lifshitz permeability argument: large permittivity begets high-frequency magnetism. *Proc. Natl Acad. Sci. USA* **106,** 1693–1698 (2009).
4. Shvets, G. & Urzhumov, Y. A. Engineering the electromagnetic properties of periodic nanostructures using electrostatic resonances. *Phys. Rev. Lett.* **93,** 243902 (2004).
5. Liu, N., Fu, L., Kaiser, S., Schweizer, H. & Giessen, H. Plasmonic building blocks for magnetic molecules in three-dimensional optical metamaterials. *Adv. Mater.* **20,** 3859–3865 (2008).
6. Alù, A., Salandrino, A. & Engheta, N. Negative effective permeability and left-handed materials at optical frequencies. *Opt. Express* **14,** 1557–1567 (2006).
7. Podolskiy, V., Sarychev, A. & Shalaev, V. Plasmon modes and negative refraction in metal nanowire composites. *Opt. Express* **11,** 735–745 (2003).
8. Luk'yanchuk, B. *et al.* The Fano resonance in plasmonic nanostructures and metamaterials. *Nature Mater.* **9,** 707–715 (2010).
9. Hao, F. *et al.* Symmetry breaking in plasmonic nanocavities: subradiant LSPR sensing and a tunable Fano resonance. *Nano Lett.* **8,** 3983–3988 (2008).
10. Verellen, N. *et al.* Fano resonances in individual coherent plasmonic nanocavities. *Nano Lett.* **9,** 1663–1667 (2009).
11. Francescato, Y., Giannini, V. & Maier, S. A. Plasmonic systems unveiled by Fano resonances. *ACS Nano* **6,** 1830–1838 (2012).
12. Brown, L. V., Sobhani, H., Lassiter, J. B., Nordlander, P. & Halas, N. J. Heterodimers: plasmonic properties of mismatched nanoparticle pairs. *ACS Nano* **4,** 819–832 (2010).
13. Yuan, H-K. *et al.* A negative permeability material at red light. *Opt. Express* **15,** 1076–1083 (2007).
14. Shalaev, V. M. Optical negative-index metamaterials. *Nature Photon.* **1,** 41–48 (2007).
15. Pendry, J. B. Negative refraction makes a perfect lens. *Phys. Rev. Lett.* **85,** 3966–3969 (2000).
16. Pendry, J. B., Holden, A. J., Robbins, D. J. & Stewart, W. J. Magnetism from conductors and enhanced nonlinear phenomena. *IEEE Trans. Microwave Theor. Tech.* **47,** 2075–2084 (1999).
17. Zhou, J. *et al.* Saturation of the magnetic response of split-ring resonators at optical frequencies. *Phys. Rev. Lett.* **95,** 223902 (2005).
18. Alù, A. & Engheta, N. Dynamical theory of artificial optical magnetism produced by rings of plasmonic nanoparticles. *Phys. Rev. B* **78,** 085112 (2008).
19. Fan, J. A. *et al.* Fano-like interference in self-assembled plasmonic quadrumer clusters. *Nano Lett.* **10,** 4680–4685 (2010).
20. Fan, J. A. *et al.* DNA-enabled self-assembly of plasmonic nanoclusters. *Nano Lett.* **11,** 4859–4864 (2011).
21. Fan, J. A. *et al.* Self-assembled plasmonic nanoparticle clusters. *Science* **328,** 1135–1138 (2010).
22. Sheikholeslami, S. N., García-Etxarri, A. & Dionne, J. A. Controlling the interplay of electric and magnetic modes via Fano-like plasmon resonances. *Nano Lett.* **11,** 3927–3934 (2011).
23. Baur, C. *et al.* Nanoparticle manipulation by mechanical pushing: underlying phenomena and real-time monitoring. *Nanotechnology* **9,** 360–364 (1998).
24. Kim, S., Shafiei, F., Ratchford, D. & Li, X. Q. Controlled AFM manipulation of small nanoparticles and assembly of hybrid nanostructures. *Nanotechnology* **22,** 115301 (2011).
25. Junno, T., Deppert, K., Montelius, L. & Samuelson, L. Controlled manipulation of nanoparticles with an atomic force microscope. *Appl. Phys. Lett.* **66,** 3627–3629 (1995).
26. Prodan, E., Radloff, C., Halas, N. J. & Nordlander, P. A hybridization model for the plasmon response of complex nanostructures. *Science* **302,** 419–422 (2003).
27. Esteban, R., Borisov, A. G., Nordlander, P. & Aizpurua, J. Bridging quantum and classical plasmonics with a quantum-corrected model. *Nature Commun.* **3,** 825 (2012).
28. Papas, C. H. *Theory of Electromagnetic Wave Propagation* (Dover, 1988).

Acknowledgements

The authors thank Chihhui Wu and Jiming Bao for helpful discussions. This work was supported in part by the US Army Research Laboratory and the US Army Research Office (W911NF-11-1-0447), the National Science Foundation (NSF; DMR-0747822), the Office of Naval Research (ONR; N00014-08-1-0745), the Air force Office of Scientific Research (AFOSR; FA9550-10-1-0022), the Welch Foundation (F-1662), the Alfred P. Sloan Foundation, AFOSR with the Young Investigator Program (YIP) (award no. FA9550-11-1-0009) and an ONR MURI grant (no. N00014-10-1-0942).

Author contributions

F.S. performed the experiments. F.M. and K.L. conducted the calculations and theoretical modelling. T.H. and X-X.L. facilitated the experimental and theoretical work, respectively. A.A and X.L. supervised the project. All authors discussed the results and commented on the paper.

Additional information

Supplementary information is available in the online version of the paper. Reprints and permission information is available online at http://www.nature.com/reprints. Correspondence and requests for materials should be addressed to A.A. and X.L.

Competing financial interests

The authors declare no competing financial interests.

ERRATUM

A subwavelength plasmonic metamolecule exhibiting magnetic-based optical Fano resonance

Farbod Shafiei, Francesco Monticone, Khai Q. Le, Xing-Xiang Liu, Thomas Hartsfield, Andrea Alù and Xiaoqin Li

Nature Nanotechnology http://dx.doi.org/10.1038/nnano.2012.249 (2013); published online 27 January 2013;
corrected after print 1 February 2013.

In the version of this Letter originally published online, the surname of the fifth author should have read 'Hartsfield'. This error has been corrected in the HTML and PDF versions of the Letter.